



Thermal and thermo-hydraulic behaviour of alumina-graphene hybrid nanofluid in minichannel heat sink: An experimental study

Vivek Kumar¹ | Sumit Kr. Singh¹ | Vikash Kumar¹ | Wasim Jamshed²  | Kottakkaran Soopy Nisar³ 

¹Department of Mechanical Engineering, Indian Institute of Technology (B.H.U.), Varanasi, India

²Department of Mathematics, Capital University of Science and Technology (CUST), Islamabad, Pakistan

³Department of Mathematics, College of Arts and Sciences, Wadi Aldawaser, Prince Sattam Bin Abdulaziz University, Wadi ad-Dawasir, Saudi Arabia

Correspondence

Kottakkaran Soopy Nisar, Department of Mathematics, College of Arts and Sciences, Wadi Aldawaser, Prince Sattam Bin Abdulaziz University, Wadi ad-Dawasir, Saudi Arabia.
Email: n.soopy@psau.edu.sa

Vivek Kumar, Department of Mechanical Engineering, Indian Institute of Technology (B.H.U.), Varanasi, India.
Email: vivekkr.rs.mec15@itbhu.ac.in

Summary

Thermal and pressure drop aspects of a minichannel heat sink have been investigated experimentally using distilled water as base fluid with alumina, graphene and alumina-graphene hybrid composition at 0.01% volume concentration. The reasons to select alumina-graphene as a potential nanomaterials combination for hybrid nanofluids are as: (i) thermal conductivity enhancement and (ii) to investigate the effect of morphology (shape and size of nanoparticles). Alumina (Al_2O_3) is oxide and has spherical shape whereas graphene is allotrope of carbon and has platelet shape. To examine the effect of different nanoparticles (in terms of shape, size and properties) dispersed hybrid nanofluid on hydrothermal behaviour is an interesting study. Effects of Reynolds number (80-450), flow rate (0.1-0.5 L/min) and fluid inlet temperature (20-40°C) are studied. The effects of uniform heat flux of 50 and 66.7 W/cm² on hydrothermal behaviour of a minichannel are also examined. The increment in convective heat transfer coefficient (*HTC*) is 30.93% at 30°C with graphene/water composition nanofluid than water base fluid. A penalty of 23.82% has been observed in pressure drop with graphene/water nanofluid over base fluid. As inlet temperature increases, Nusselt number (*Nu*) increases while adverse effect is found in case of friction factor. Performance evaluation criteria (*PEC*) has been observed more than 1 for all nanofluids and hybrid nanofluids, which ensured that nanofluids act as a better electronic cooling agent than water. Al_2O_3 + graphene hybrid nanofluid delivers optimum comparison factor (*HTC* to pressure drop ratio) and lower entropy generation rate among used working fluids. Graphene/water nanofluid yields less comparison factor compared to other working fluids irrespective of high *HTC*. $h/\Delta p$ is favourable for nanofluid of unlike particles of hybrid composition (in terms of particle size, properties and shape) as compared to mono nanofluid and hybrid nanofluid having similar particles.

KEYWORDS

entropy generation, *HTC* and pressure drop ratio, hybrid nanofluid, minichannel, *PEC*, Nusselt number

1 | INTRODUCTION

Energy systems such as motors, microelectronic applications, batteries, micro reactors, etc., required an effective cooling system due to miniaturisation. Very high heat fluxes can be removed easily using a micro/minichannel heat sink installation.^{1,2} Thus, for optimal performance of a miniature component, its thermal management is necessary and methods for heat transfer improvement classified mainly as active, passive and hybrid techniques.³⁻⁶ External energy (mechanical, surface vibration and electrostatic fields) comes under active techniques. A disturbed flow was created by incorporating rough and extended surfaces, swirl and unconventional fluids is part of the passive method. Meanwhile, a combined active and passive techniques cumulatively called as compound or hybrid method. Complicated design limits application of compound method. Furthermore, from literature, passive technique performs better in heat transfer enhancement compared to other two available techniques.^{4,5} The miniaturised heat exchanger is a feasible option for a decade due to its capability to preserve materials, space constraints and efficient cooling. Due to this, miniaturised heat exchanger is able to transmit more heat compared to an ordinary heat exchanger. The microchannel heat sink (MCHS) has been the subject of numerous investigations in recent decades due to its performance.⁷⁻¹⁰ Due to higher energy density requirements, better thermophysical characteristics of cooling agent is necessary to release the excess energy. Therefore, nanofluid and hybrid composition nanofluid have come as alternative fluid due to their better thermo-hydraulic attributes.^{11,12} In the literature, it is available that hybrid nanofluid possesses superior thermo-hydraulic performance than mono nanofluid.¹³ The researchers have paid attention to alumina, which is the most common metal oxide nanoparticle. It has lower cost, higher heat transfer coefficient (*HTC*), better stability and availability to compare increased pumping power.¹⁴ On the other hand, graphene nanoparticle holds better heat conductivity and high specific surface area, leading to improved heat transfer. Thus, for the same of heat transfer scale, less demand for heat transfer fluid and pumping power is needed.¹⁵ Therefore, alumina and graphene combination may be the best candidate in hybrid nanofluid for mini/microchannel heat sink (MCHS).

In the literature, various investigations on mini/microchannel heat sink (MCHS) are available for thermo-hydraulic characteristics using nanofluid experimentally and numerically.¹⁵⁻²² However, few literatures are there on MCHS thermo-hydraulic performance using hybrid nanofluid as a cooling agent. Ho et al²³⁻²⁵ performed experimental analysis of MCHS with water

based hybrid nanofluid. They revealed that at higher Reynolds number, Al_2O_3 /water nanofluid performs better than the Al_2O_3 + MEPCM hybrid-based nanofluid. Authors also reveal that the flow rate is a critical parameter for the cooling effectiveness of the nanofluid and claimed an optimum data under which suspension system performs appreciably better than mono-particle based nanofluid due to synergistic influence of the Al_2O_3 and PCM suspension both. An enhancement of 12.61% and 24.35% was observed by Selvakumar and Suresh²⁶ for pumping power and heat transfer coefficient in minichannel, respectively. Ahammed et al²⁷ reported an enhancement of 63.13% in convective coefficient in a minichannel using graphene-alumina hybrid nanofluid. Hussien et al²⁸ performed an experimental analysis on microtubes passage using a coolant MWCNTs/GNPs hybrid composition nanofluids and revealed a net 58% improvement in heat transfer coefficient. They²⁹ also studied Al_2O_3 + graphene hybrid nanofluid flow through minitubes, numerically. The optimum increment of 13.7% was found in *HTC* for Al_2O_3 + graphene hybrid composition nanofluid over Al_2O_3 /water nanofluid. Nimmagadda and Venkatasubbaiah³⁰ performed an experimental study in microchannel using Al_2O_3 + Ag hybrid composition nanofluid and claimed that nanoparticles fraction increment resulted in Nusselt number enhancement. CNT/ Fe_3O_4 hybrid nanofluid, at low fraction Fe_3O_4 , showed a peak point value of total entropy generation within a minichannel heat exchanger.³¹ The numerical investigations for different configured microchannel heat sink in laminar regime^{32,33} using graphene-Ag hybrid nanofluid showed that nanofluid results in a better cooling agent than water. Figure of merit is always more than 1.5 in chaotic twisted minichannel with hybrid nanofluid composed of graphene and platinum.³⁴ Shahsavari et al³⁵ investigated a double pipe minichannel with coolant as Fe_3O_4 /CNT/water hybrid composition nanofluid and numerically studied fluid behaviour as newtonian and non-Newtonian. They also studied the hydrothermal behaviour of fluid in the minichannel and found that Newtonian hybrid composition nanofluid has better effectiveness, overall *HTC* and heat transfer rate than non-Newtonian hybrid nanofluid. Uysal et al³⁶ selected a Fe_3O_4 -diamond/water hybrid composition nanofluid used in a flat tube type minichannel and numerically presented that hybrid composition nanofluid has elevated convection *HTC* and Nusselt number than mono nanoparticles used. Ho et al³⁷ investigated experimentally on nano-encapsul phase change materials (NEPCMs) in MCHS. They discovered that NEPCMs-particles show high performance up to 70%. Kumar and Sarkar^{38,39} experimentally analyzed thermohydraulic performance and also effect of

coolant inlet temperature in a minichannel heat sink and suggested that coolant entry temperature has significant heat transfer improvement of a heat sink. Nanofluid as heat transfer medium utilise in several application as in compact heat exchanger, solar applications, micro passages and channels for heat transfer enhancement.⁴⁰⁻⁴³ Also, nanofluid rheological behaviour as a Newtonian and two phase non-Newtonian is well explored and its impact on flow boiling application has been analyzed.⁴⁴⁻⁴⁷ However, there are very few literatures available on graphene/water and Al_2O_3 -graphene/water hybrid nanofluids working as coolants in MCHS, but no literature available to examined the effect of fluid inlet temperature and heat flux on thermo-hydraulic characteristic of a minichannel heat sink using Al_2O_3 -graphene composed hybrid nanofluid on a single platform. It is very necessary to study the relative influence of *HTC* and pressure drop (ie, comparison factor)^{48,49} for overall cooling performance of the heat sink and it is not available in previous literature of Al_2O_3 -graphene hybrid nanofluid.

Hence, based on the research gap, this experimental study aim is to analyze the performance of minichannel heat sink (MCHS) using different nanofluids at different Reynolds number (flow rates), heat flux and inlet temperature. The effects of Reynolds number, entrance temperature and heat flux were examined on the thermal characteristics (CHTC, non-dimensional parameter Nusselt number) and pressure reduction parameters (drop in pressure, friction factor). Consequent influence of *HTC* and pressure drop have been analyzed for various working medium fluids at different Reynolds number.

Performance evaluation criteria (*PEC*) and net entropy generation rate impact on various working coolants are also presented in the paper.

2 | METHODOLOGY

2.1 | Experimental facility

The fluid flow circulation loop and the experimental setup are illustrated in Figures 1 and 2, respectively. The test section can be easily engaged and disengaged. Detail dimensional description of the test section is given in Reference 38. The heat sink is made up of nine minichannels measuring 30 mm in length, 3 mm in height and 1 mm in width. The picture and layout of a minichannel heat sink are shown in Figure 3. On bottom of the heat sink, three cartridge heater of maximum power 150 W has been applied to provide constant heat fluxes of 50 and 66.67 W/cm^2 . To restrict heat loss from heat sink to surrounding, insulation is used and data acquisition system used to record the data. Dimension values of $\pm 0.02 \text{ mm}$, temperature of $\pm 0.1^\circ\text{C}$, drop in pressure of $\pm 0.25\%$ flow rates of $\pm 0.5\%$ and heating power sources of $\pm 0.25\%$ uncertainties.

The experiments were performed with distilled water, Al_2O_3 /water, graphene/water nanofluid and Al_2O_3 -graphene/water (50:50, v/v) hybrid nanofluid. A pump was used to proper supply of coolants at different entrance temperatures successfully at 20°C , 30°C and 40°C conditions from the tank. The heat power was provided to the system after constant flow rate has been maintained. Two

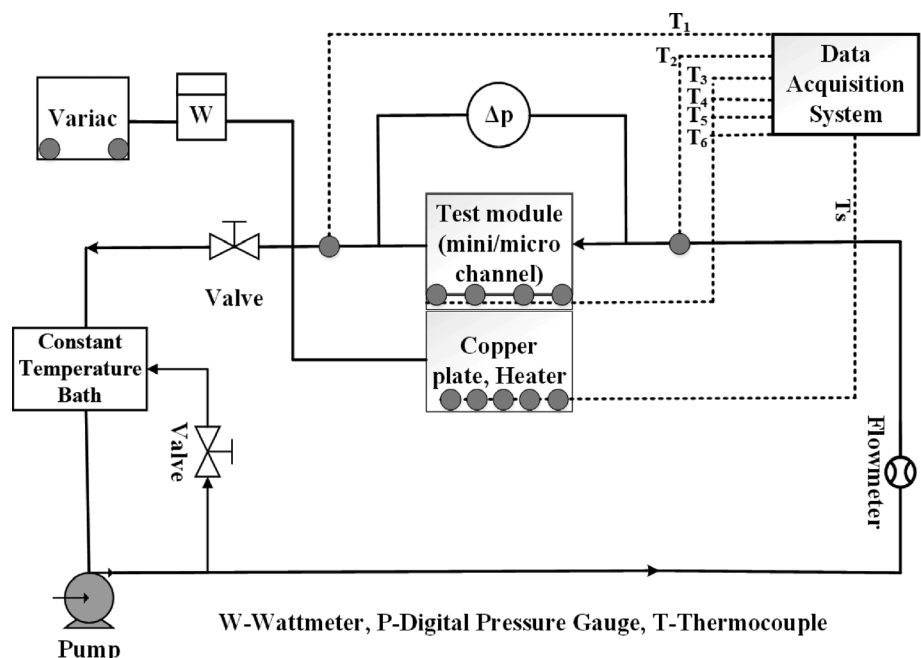


FIGURE 1 Schematic of desired work³⁸



FIGURE 2 Experimental setup of the present study³⁸

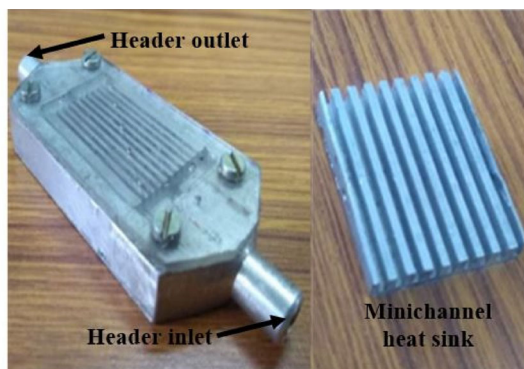


FIGURE 3 Actual and schematic image of minichannel heat sink³⁹

different heat flux 50 and 66.7 W/cm² were considered for the present study. Five thermocouples were located at different positions (four thermocouples at the minichannel corners and immediate one at core centre) of heat sink at bottom to calculate the surface temperature (T_{tc}). The

parameters (flow rate of nanofluid, bottom heat flux and nanofluid inlet temperature) were kept unvaried for each measurement. However, after 40-45 minutes, a steady-state condition was reached, with very minor temperature fluctuations ($\sim 0.0002^\circ\text{C}/\text{h}$). As a result, the temperature was expected to be constant throughout the procedure and no need to compensate the effect of response time delay of thermocouples. By averaging of five readings, surface temperature of heat sink (T_{tc}) is obtained. Average surface temperature measured during the experiment was in the range of 65.4°C to 52.3°C. As the flow rate increased, the temperature of base of heat sink reduced.

2.2 | Nanofluids preparation

Water-based nanofluids and Al₂O₃-graphene hybrid nanofluid were prepared using two-step method. Alumina nanoparticles (45 nm) and graphene nanoplates (thickness: 7 nm, diameter: 5-10 μm) were purchased by Alfa Aesar, USA and Otto Chemie Pvt. Ltd., respectively. To prepare nanofluids, calculated amount of Al₂O₃ and graphene nanoparticles were measured by an weighing machine (SHIMADZU, ATX224, Japan) and suspended in distilled water. An ultrasonic device was used for 7 hours to disrupt the cells and homogenise the colloidal solution with no surfactant. The stability of prepared nanofluids was observed for more than 3 days.

The obtained range of pH value is in the range of 7.83-7.86 taken from the different locations of a given sample of nanofluids. To ensure stability and uniformity of the prepared solution, isoelectric point was analyzed and pH of the solution remained away from the stated isoelectric point (IEP).⁵⁰ As there is strong repulsive force among the particles, better stability and uniformity is attained for nanofluids having pH value far off from IEP. The same given samples were used to measure the viscosity and density of nanofluids. No significant difference was obtained in the viscosity and density of all samples. A 99% degree of homogeneity was assured on the basis of measured properties for a given sample of nanofluids.

2.3 | Thermo-physical properties of nanofluids

Table 1 shows the thermophysical characteristics of working fluids at 30°C. Nanofluids and water properties were measured using various equipment. Thermal properties mainly fluid conductivity and specific heat capacity were measure out from a Hot disk instrument. Before data collection, the instrument was well calibrated and rehearsed three times. Viscosity of samples were measure out using an LVDV-II + Pro Brookfield digital viscometer. Density was estimated by ratio of mass upon volume after determining mass by digital weighing machine and volume by measuring container. Heat capacity (ρc_p) value was measured directly from the hot disk analyser of TPS-500 version and the heat capacity was determined using ratio of ρc_p to ρ .

2.4 | Data analysis

Heat transfer rate in MCHS is calculated by,

$$\dot{Q} = \dot{V} \rho c_p (T_{out} - T_{in}) \quad (1)$$

The average heat transfer coefficient was defined by,

$$h = \frac{\dot{Q}}{A(LMTD)} \quad (2)$$

where LMTD defines the change in wall temperature and fluid average temperature. It is given by,^{20,51}

$$LMTD = \frac{(T_w - T_{in}) - (T_w - T_{out})}{\ln\left(\frac{T_w - T_{in}}{T_w - T_{out}}\right)} \quad (3)$$

T_w represents the channel wall temperature. It is measured by 1D heat transfer in a minichannel planes and thermocouples. It is calculated as,⁵¹

$$T_w = T_{tc} - \left(\frac{\dot{Q} h_w}{k_s A_b}\right) \quad (4)$$

where T_{tc} is the average of five thermocouples temperature which are inserted at the bottom of the minichannel to measure temperature. h_w is the separation length of thermocouple and heat sink wall surface, which is 6 mm. k_s is the thermal conductivity of material of heat sink. Heat sink is of aluminium material having thermal conductivity of 235 W/m² K. A_b is the base area, which is calculated as,

$$A_b = WL \quad (5)$$

where W and L are consequent width and length of the design minichannel heat sink. The effective area (A) for heat transfer is given by,

$$A = N \left(w_{ch} + 2\eta_{fin} h_{ch} \right) L_{ch} \quad (6)$$

where η_{fin} is fin efficiency and iterative method is used to find out the fin efficiency using Equations (7) and (8).⁵²

$$\eta_{fin} = \frac{\tanh(mh_{ch})}{mh_{ch}} \quad (7)$$

$$m = \sqrt{2h/(k_s w_{fin})} \quad (8)$$

Hydraulic diameter (d_h) of minichannel is calculated as,

$$d_h = \frac{2w_{ch} h_{ch}}{w_{ch} + h_{ch}} \quad (9)$$

TABLE 1 Properties of distilled water and various nanofluid at temperature (30°C)

Different fluid	k (W/m K)	ρ (kg/m ³)	c_p (J/kg K)	μ (Pa s)
Distilled water	0.6171	997.4	4182.5	0.00092
Al ₂ O ₃ /water	0.6175	998.8	4181.0	0.00093
Al ₂ O ₃ + graphene (50:50)/water	0.6181	998.6	4180.9	0.00098
Graphene/water	0.6194	998.3	4180.7	0.00104

Thus, the Nusselt number is determined by,

$$Nu = \frac{hd_h}{k} \tag{10}$$

Mean fluid velocity u_m is defined as,

$$u_m = \frac{\dot{V}}{Nw_{ch}h_{ch}} \tag{11}$$

The Reynolds number is calculated as,

$$Re = \frac{\rho u_m d_h}{\mu} \tag{12}$$

The friction factor is calculated as,

$$f = \frac{2d_h \Delta p}{L_{ch} \rho u_m^2} \tag{13}$$

The comparison factor, J , which is a ratio of HTC to Δp , is used to investigate the combined effect of HTC and Δp owing to the application of nanoparticles.⁴⁸ It is given by,

$$J = \frac{h}{\Delta p} \tag{14}$$

Performance evaluation criteria (PEC) is calculated as,³⁹

$$PEC = \frac{Nu_{nf}/Nu_{bf}}{(f_{nf}/f_{bf})^{1/3}} \tag{15}$$

Consider the heat sink as a thermal system. Fluid flow process in the thermal systems consists of mainly two types of irreversibility due to heat transfer mechanism and pressure drop. Net entropy generation rate within the minichannel is determined using entropy balance method in control volume of thermal system.⁵³

$$S_{in} + dS_{gen} + \left(\frac{d\dot{Q}}{T_s}\right) = S_{out} \tag{16a}$$

where S_{in} , S_{out} , T_s and S_{gen} are the entropy inlet, entropy outlet, surface temperature and entropy generation in the system, respectively.

$$dS_{gen} = (S_{out} - S_{in}) - \left(\frac{d\dot{Q}}{T_s}\right) \tag{16b}$$

$$d\dot{Q} = \dot{m} c_p dT \tag{17}$$

By considering the working fluid as incompressible fluid (ie, the density of working fluid constant) and all other properties constant throughout the process. Equation (16b) is converted for a control volume and given as,

$$\dot{S}_{out} - \dot{S}_{in} = \int \dot{m} \left(c_p \frac{dT}{T} - \frac{dp}{\rho T} \right) = \int d\dot{S}_{gen} + \int \frac{\delta \dot{Q}}{T_s} \tag{18}$$

In Equation (18), T_s is defined as the heat sink's surface temperature, which is measured by thermocouples and after steady-state condition so, T_s is assumed as constant. By Integration Equation (18) between inlet and outlet of the heat sink, the total entropy generation rate is calculated as follows,⁵⁴

$$S_{gen} = \dot{m} \left[c_p \ln \left(\frac{T_{out}}{T_{in}} \right) - \frac{(p_{out} - p_{in})}{\rho T_m} \right] - \left(\frac{\dot{m} c_p (T_{out} - T_{in})}{T_s} \right) \tag{19}$$

$$S_{gen} = \dot{m} \left[c_p \ln \left(\frac{T_{out}}{T_{in}} \right) + \frac{\Delta p}{\rho T_m} \right] - \left(\frac{\dot{Q}}{T_s} \right) \tag{20}$$

where T_m represents mean temperature and determined by $T_m = (T_{in} + T_{out})/2$.

2.5 | Uncertainty evaluation

Uncertainty of the different variables has been evaluated by available equation given by Kline and McClintock.⁵⁵ Equation consists R which is a function of independent parameters $X_1, X_2, X_3, \dots, X_n$, while $W_1, W_2, W_3, \dots, W_n$ are related uncertainties. Uncertainty of dependent variables as HTC, Q, f , etc., is W . Uncertainty values evaluated of respective variables are shown in Table 2.

$$W = \left[\left(\frac{\partial R}{\partial X_1} W_1 \right)^2 + \left(\frac{\partial R}{\partial X_2} W_2 \right)^2 + \dots + \left(\frac{\partial R}{\partial X_n} W_n \right)^2 \right]^{1/2} \tag{21}$$

3 | VALIDATION

Experimental test section run has been verified and its reliability justification has been done by research work.³⁸ Also, the data for conventional fluid (water) has been shown in the research paper. For the validation part, the

TABLE 2 The uncertainties of the measured experimental variables

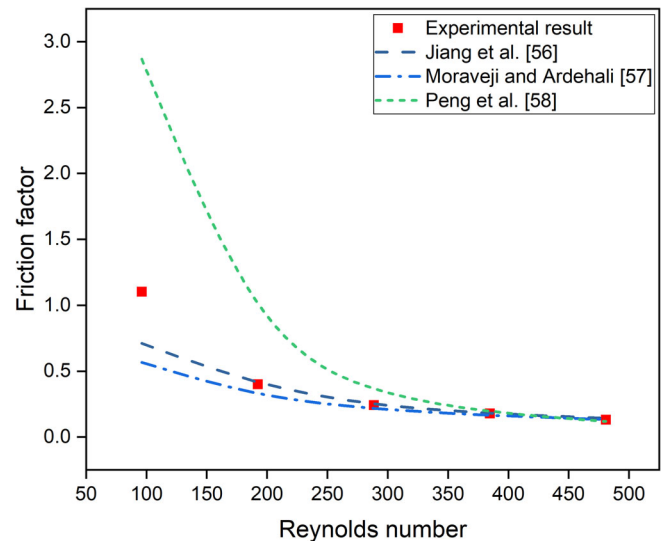
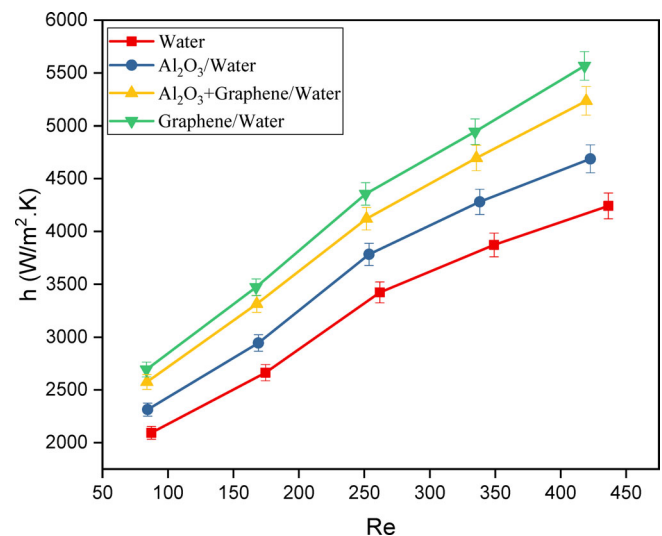
Variables	Uncertainty values (%)
\dot{Q} (W)	± 2.86
A (m ²)	± 1.3
d_h (m)	± 1.02
\dot{V} (L/min)	± 0.5
u_m (m/s)	± 0.77
Δp (Pa)	± 0.25
k (W/m K)	± 2.0
μ (Pa/s)	± 2.0
ρ (kg/m ³)	± 2.0
c_p (J/kg K)	± 2.0
HTC, h (W/m ² K)	± 2.9
f	± 2.69
Re	± 3.1
PEC	± 5.57
Nu	± 3.82
$h/\Delta p$	± 3.12

Nusselt number determined experimentally was compared from the existing correlations for Nusselt number determined by different authors.³⁸ In Figure 4, the experimental friction factor for MCHS with DI water is compared to the available literature correlations.^{56–58} Except for the variance at low Reynolds numbers, the experimental results of friction factor matched the available correlation of Jiang et al⁵⁶ the best. When $Re > 190$, there is no substantial variance. This deviation is due to some reasons as mismatch in geometry, aspects and situations that were used to build correlations.

4 | RESULTS AND DISCUSSIONS

4.1 | Effects on heat transfer performance

Figure 5 demonstrates the impact of Reynolds number on HTC with the working fluids applied at 30°C. Also, heat flux and entrance temperature dependency on HTC have been plotted in Figure 6 at particular flow rate of 0.3 L/min (equivalent to Re 250) for different working fluids. The Reynolds number for nanofluid is different from the Reynolds number for water in Figures 5, 7, and 9, etc. As defined in Equation (12), Reynolds number is directly proportional to density and inversely proportional to dynamic viscosity. The variation is due to change in the properties

**FIGURE 4** Comparisons of friction factor**FIGURE 5** Heat transfer coefficient variation with Re for different fluids ($T_{in} = 30^\circ\text{C}$)

(density and dynamic viscosity) of nanofluids after suspending the nanoparticles. So, the variation in Reynolds number is coming due to change in properties in case of nanofluids. The constant temperature is maintained at the entrance of the MCHS by using constant temperature bath (chiller). In the figures, results have been presented for various working fluids as Al_2O_3 /water, graphene/water and hybrid nanofluid $\text{Al}_2\text{O}_3 + \text{graphene}$ /water synthesized for total volume concentration of 0.01%.

The figure reveals that HTC rises with increases in Reynolds number. The diminishing in thermal boundary thickness, nanoparticles Brownian motion, thermal conductivity rise, thermophoresis effect and the effect of nano-fins contribute to enhancement in HTC .^{14,59} Also,

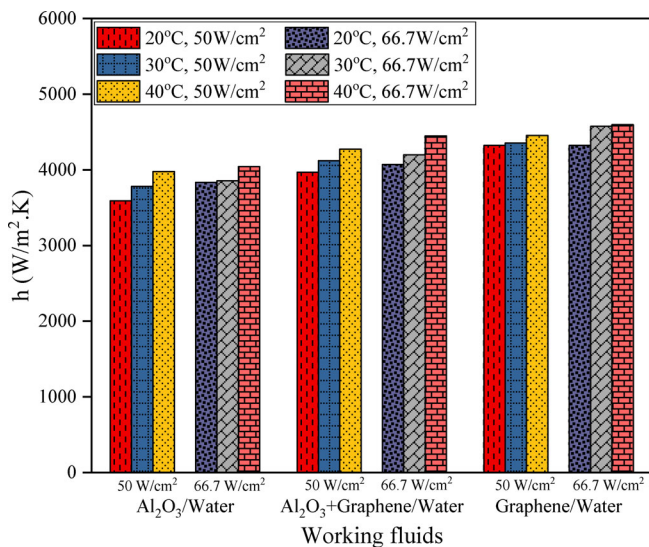


FIGURE 6 Influence of various entrance temperature and heat flux on heat transfer coefficient for different working fluids at 0.3 L/min

another effect is the particles' mobility, which is due to their small size and may result in micro-convection around particles in fluid and hence greater heat transmission through the nanofluids within minichannel. Many authors claimed micro-convection in nanofluids and the positive effect of micro-convection on heat transfer.⁶⁰ The boundary layer may be diminished due to decreased viscosity caused by higher temperature. Thermal boundary layer reduction improves heat transfer coefficient at the same temperature change. Surface area to volume of the nanoparticles is more which transports the heat transfer within the medium rapidly. The *HTC* is augmented on graphene particles addition. The highest value of *HTC* was exhibited by graphene/water nanofluid of 5656.33 W/m² K. The maximum enhancement was calculated nearly 30.93% for 0.01 vol% graphene based nanofluid. This is due to very high heat conductivity and high specific surface area to volume ratio of graphene nanoparticles.¹⁵ It exhibits from Figure 6 that fluid inlet temperature and heat flux have a significant influence on *HTC* at 0.3 L/min. An increment in the range of 3.9%–6.8% found for heat transfer coefficient with all working fluid when temperature increases from 20°C to 40°C. At elevated temperature, heat transfer enhancement was significant due to better nanofluids thermal properties. However, heat transfer coefficient enhancement dependency on fluid inlet temperature stated in previous literature.³⁹ They also showed the same influence of nanofluid entrance temperature on heat transfer coefficient. Thus, thermal conductivity of working fluid becomes more significant at larger temperatures. Whereas *HTC* increases

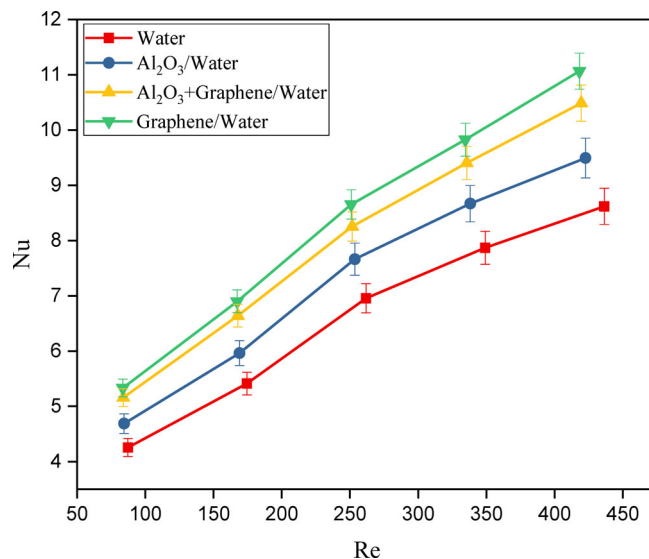


FIGURE 7 Nusselt number variation with Re for different fluids ($T_{in} = 30^\circ\text{C}$)

within the range of 1.9%–5.1%, when heat flux increases from 50 to 66.7 W/cm². The same impact of heat fluxes on *HTC* is revealed in the literature.⁵⁹ By increasing the heat flux, the effect of entrance temperature is observed in Al₂O₃ + graphene/water hybrid nanofluid but the impact of entrance temperature in other two nanofluids is not witnessed at same fraction. The reason to support this phenomenon is may be due to low thermal conductivity of Al₂O₃/water nanofluid and uncertainty in heat transfer coefficient.

The Nusselt number performance parameter variation with Reynolds number has depicted in Figure 7 for different working fluids at inlet temperature of 30°C. The occurrence of nanoparticles within the DI water enhances the Nusselt number. The highest value of Nusselt number is found to be 11.32 for graphene-based nanofluid. An optimum augmentation of 28.46% is observed for graphene-/water-based nanofluid than primary fluid at $Re = 435.4$. The main reason is that Reynolds number is proportionate of inlet velocity. Higher velocity leads to increased collision rate among particles which raises the heat transfer rate and thus enhances the Nusselt Number.⁴⁷ Variation in temperature, heat flux and its effect on Nusselt number has been shown in Figure 8. As seen in the illustration, Nusselt number increases with inlet temperature and heat flux. Once the coolant entry temperature reaches to 40°C from 20°C, Nusselt number enhances from 3.6% to 7.1% for all the coolants. The Nusselt number improved within the range of 2.2%–5.8% when heat flux rises from 50 to 66.7 W/cm².

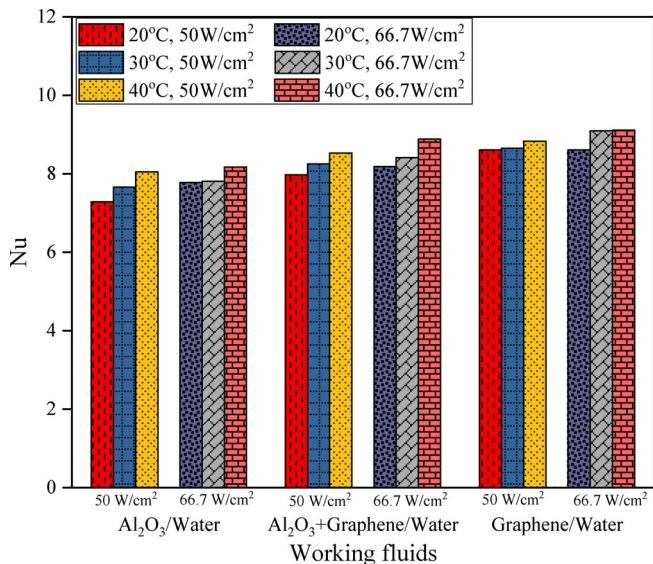


FIGURE 8 Influence of various entrance temperature and heat flux on Nusselt number for various coolants at 0.3 L/min

4.2 | Effects on pressure drop performance

Pressure drop variation with Reynolds number parameter has been illustrated in Figure 9 for the minichannel. The viscosity and density are the key factors for the rise in pressure drop due to nanoparticles dispersion. The optimum pressure drop was found 319.2 Pa for graphene/water hybrid composed nanofluid. An increase of about 23.82% was observed for graphene-based hybrid composition than base fluid (DI water). Pressure drop reduction at various entrance temperature and heat flux for coolants have been depicted in Figure 10 at the coolant flow rate of 0.3 L/min. Meanwhile, fluid entrance temperature increment causes reduction in pressure change due to drop in viscosity value with increased temperature. On increment in temperature range from 20°C to 40°C, there is reduction of pressure drop has been found in the range of 11.56%–14.45% for all the working fluids. For the same cross-section of the minichannel, pressure drop increases as the Reynolds number (flow rate) increases. Also, from Figure 9, it can be concluded that the points have more divergence at the larger Reynolds number. To support the trend, the difference in pressure drop between Al₂O₃ + graphene/water hybrid nanofluid and DI water is 13.3 Pa at the lowest Reynolds number (Re ~ 85). However, this difference is about 53.62 Pa at the highest Reynolds number (Re ~ 430) within studied range of Reynolds number. It can be justified as a known fact that rise in pressure drop depends upon the viscosity and mass flux but mass flux predominates pressure drop at elevated fluid flow rate. Meanwhile, drop in pressure

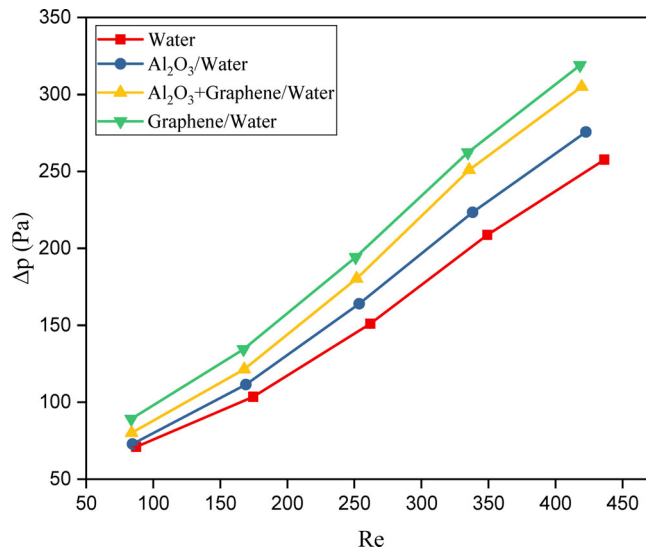


FIGURE 9 Pressure drop variation with Re ($T_{in} = 30^\circ\text{C}$)

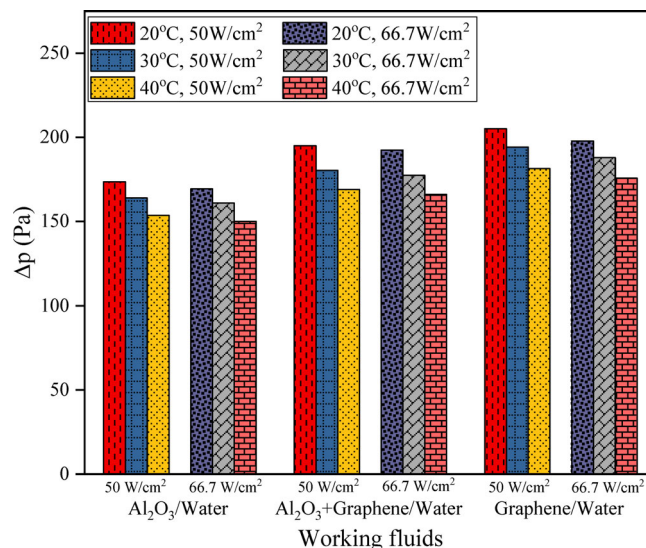


FIGURE 10 Effect of different inlet temperature and heat flux on pressure drop for different working fluids at 0.3 L/min

change occurs with increased heat flux. As heat flux increases from 50 to 66.7 W/cm², the decrement in pressure drop occurred in the range of 1.8%–2.51% for all the working fluids. But this decrement in pressure drop is not significant.

Figure 11 illustrates the friction factor dependency on Reynolds number for operated coolant fluids at 30°C of entrance temperature. The impact of inlet temperature and heat flux on friction factor has been shown in Figure 12 for different nanofluids. The result reveals that a reduced friction factor with Reynolds number increment due to combined impacts of decreasing the boundary layer and mass velocity increment. Due to the

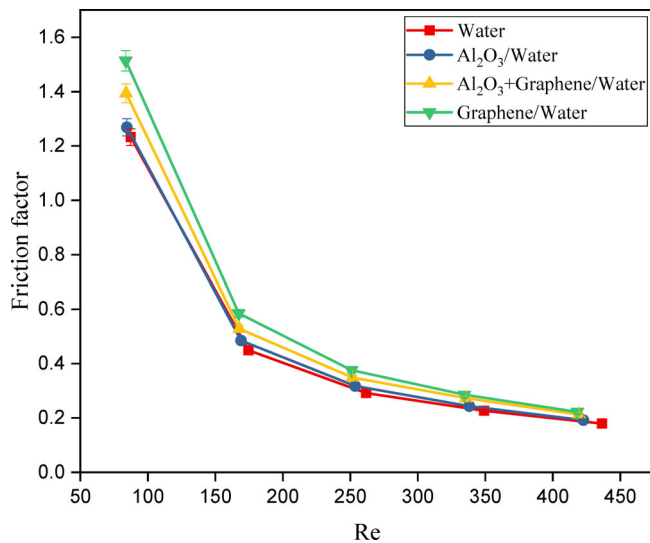


FIGURE 11 Friction factor variation with Re for different fluids ($T_{in} = 30^{\circ}C$)

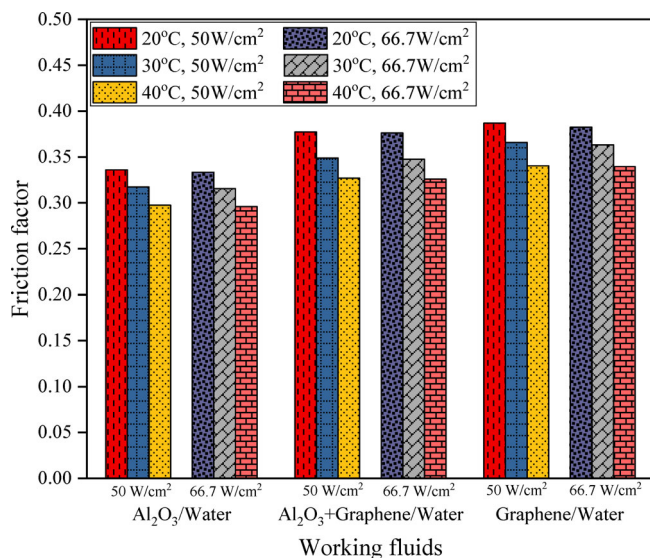


FIGURE 12 Friction factor variation with inlet temperature and heat flux for nanofluids at 0.3 L/min

presence of small particles and its well dispersion into the base fluid, the friction factor rises because of increased viscosity and slip mechanism. At $Re = 83.65$, the friction factor has maximum value of 1.51 for graphene based nanofluid. The friction factor deviates significantly at low Reynolds numbers, as shown in Figure 11. And it is due to predominance of viscosity at low Reynolds number. However, results also revealed that graphene/water nanofluid composition nanofluid has highest friction factor comparative to other coolants. It is due to increase in viscosity by suspending graphene nanoparticles which directly results in higher particle

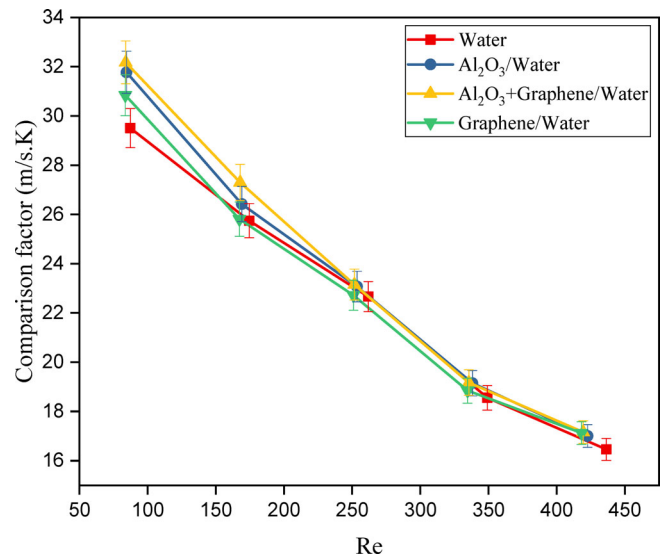


FIGURE 13 Comparison factor ($h/\Delta p$) with Re for different fluids ($T_{in} = 30^{\circ}C$)

surface area and rise in collision between them. Also, this behaviour could be due to fastest boundary layer diminishing of graphene nanofluid than other fluids. A decrement in friction factor was observed with a rise in entrance temperature but no significant change with increase in heat flux. It can be illustrated in Figure 12. Same trend has been represented by the friction factor as pressure drop when the effect of inlet temperature and heat flux have taken into account on friction factor.

4.3 | Relative effect on HTC and pressure drop (ie, comparison factor)

Figure 13 represents the Reynolds number effects on the thermo-fluid ratio, that is, comparison factor, which is ratio of convective HTC and the pressure drop ($h/\Delta p$) determined for all working fluids. The comparison factor is used to investigate the combined effect of h and Δp caused by nanoparticle application. Gao et al⁴⁹ has decided that what heat sink is overall best in performance based on the comparative effect of h and Δp . It is observed that this ratio has maximum value at low Reynolds number due to HTC increases rapidly compared to pressure drop. $h/\Delta p$ ratio decreases with rising in Reynolds number. $Al_2O_3 +$ graphene/water hybrid nanofluid has highest value for $h/\Delta p$ ratio. $h/\Delta p$ ratio is for graphene/water nanofluid very less regardless of high convective HTC . Even, $h/\Delta p$ ratio is less for graphene/water nanofluid as compared to Al_2O_3 /water nanofluid. The main reason is high drop in pressure because of the high graphene nanoplates surface area. The curve for

graphene/water nanofluid intercepts the curves of other working fluids as a result of higher increment in pressure drop when compared to heat transfer coefficient for graphene/water nanofluid at high Reynolds number. So, it can be claimed that hybrid composition nanofluids having dissimilar particles in terms of shape, size and properties have favourable comparison factor as compared to mono nanofluids and hybrid nanofluid contains similar nanoparticles.^{38,39}

The impact of inlet temperature and heat flux on comparison factor ($h/\Delta p$) ratio has been represented in Figure 14. From the figure, it has been shown that $h/\Delta p$ ratio hikes with rise in entrance temperature and heat flux. The reason is that HTC increases and pressure drop reduces when inlet temperature increases from 20°C to 40°C and heat flux increases 50 W/cm² to 66.7 W/cm². It has been discussed above in the text. $h/\Delta p$ ratio rises in the range of 15.81% to 24.28% when temperature increases from 20°C to 40°C for all working fluids. A maximum enhancement of 24.28% in $h/\Delta p$ ratio was found for Al₂O₃ + graphene/water hybrid nanofluid. When heat flux rises from 50 to 66.7 W/cm², an enhancement in the range of 3.5% to 9.47% has been observed for all working fluids. From all the working fluids, Al₂O₃ + graphene/water hybrid nanofluid has better comparison factor.

4.4 | Performance evaluation criteria (PEC)

However, to estimate the thermal efficiency of minichannel, the term PEC has been determined.

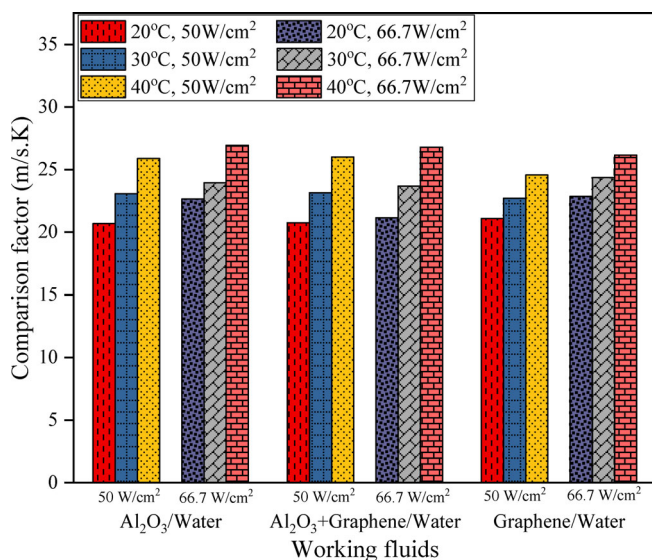


FIGURE 14 Effect of different inlet temperature and heat flux on comparison factor ($h/\Delta p$) for different working fluids at 0.3 L/min

Influence of Reynolds number with PEC for various working fluids has depicted in Figure 15. PEC value is found greater than unity among the cases studied, which indicates that using nanofluid can be considered a better option to be used as coolant than water in MCHS. Also, results revealed that HTC is predominant over enhancement in the pressure drop. PEC first decreases and then starts to rise on Reynolds number increment. Optimum PEC value was observed to be 1.198 for graphene/water nanofluid at $Re = 420$. Fluid entrance temperature and heat fluxes effects have been represented in Figure 16 for a volumetric flow rate of 0.3 L/min. PEC value is decreased with inlet temperature but increased with the heat flux. It can be justified by that friction factor ratio (ratio of f_{nf} and f_{bf}) dominates over Nusselt number ratio (ratio of Nu_{nf} and Nu_{bf}) when the temperature rises from 20°C to 40°C, and show the opposite effect with heat flux.

4.5 | Total entropy generation rate

Net rate of entropy generation variation with Reynolds number is shown in Figure 17 for working fluids. As expected, a rise in entropy generation found on rise in Reynolds number. Optimum rate of entropy generation found for graphene based nanofluid but at higher Reynolds number growth becomes stagnant. When added the nanoparticles in base fluid, the irreversibility due to friction increases as well as the Reynolds number tends to increase the flow velocity which results in enhancing irreversibility. Overall effect ensures rise in net entropy generation rate with nanoparticles inclusion and also with flow velocity increment except in the case of Al₂O₃ + graphene/water hybrid composition nanofluid.

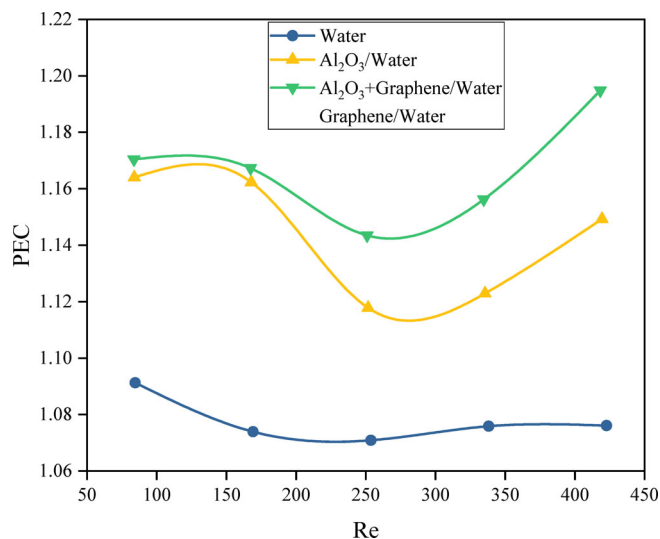


FIGURE 15 PEC with Re for different nanofluids ($T_{in} = 30^\circ C$)

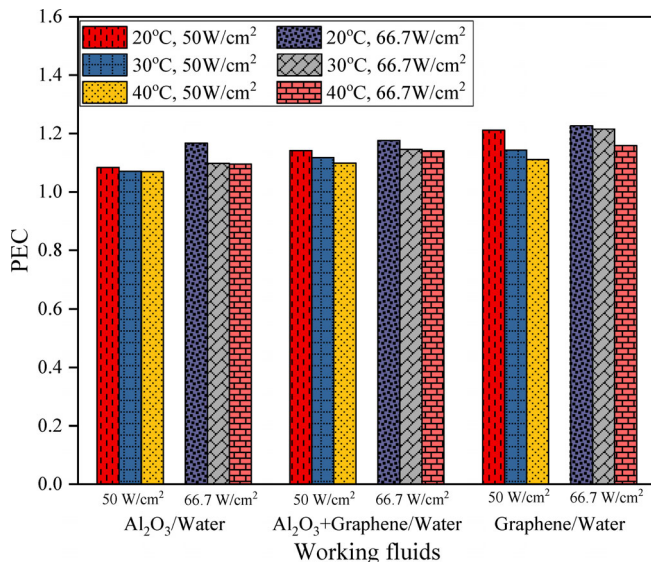


FIGURE 16 Effect of different inlet temperature and heat flux on PEC for different nanofluids at 0.3 L/min

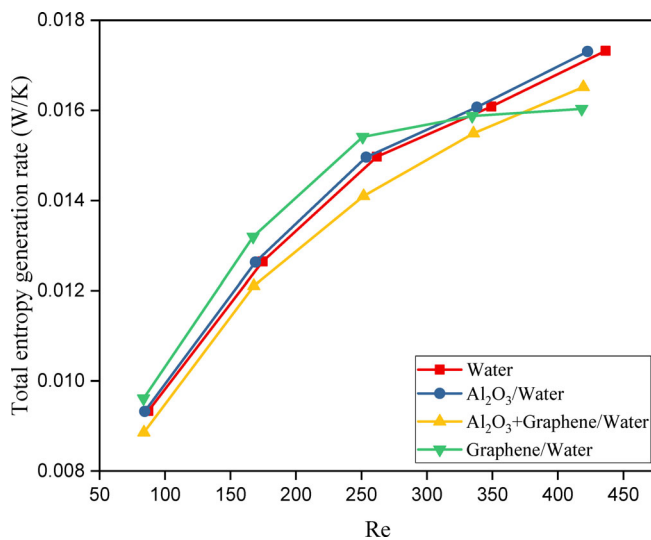


FIGURE 17 Total entropy generation rate with Re for nanofluids ($T_{in} = 30^{\circ}\text{C}$)

The curve of graphene/water nanofluid intercepts to the curves of other working fluids. The reason to support is that the irreversibility due to friction and heat transfer is approximately same for Reynolds number more than 250. The effect of different entrance temperature and heat flux on net rate of entropy generation for various working fluids has been depicted in Figure 18. Entrance temperature has shown an adverse effect on rate of entropy generation. As the temperature increases from 20°C to 40°C , thermal entropy raises while friction entropy reduces. So, it can be claimed that the friction entropy generation dominates over thermal entropy generation rate when

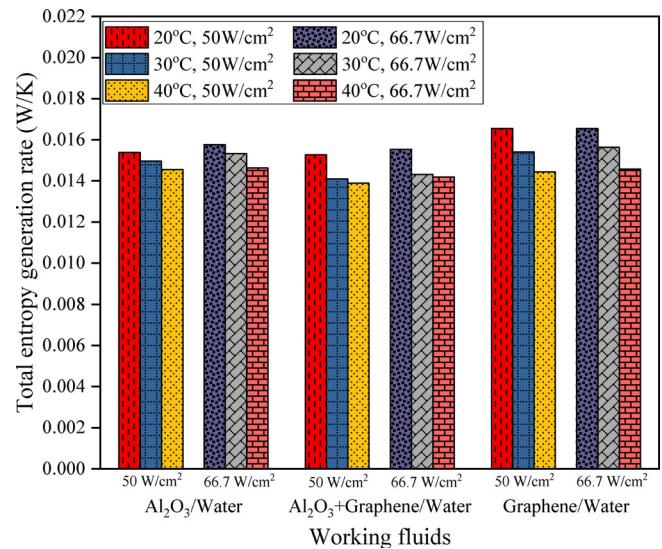


FIGURE 18 Effect of different inlet temperature and heat flux on total entropy generation rate for different working fluids at 0.3 L/min

fluid inlet temperature increases from 20°C to 40°C . But as the heat flux increases from 50 to 66.7 W/cm^2 , thermal entropy generation dominates over friction entropy generation. So, from Figure 18, it can be shown that as the heat flux increases from 50 to 66.7 W/cm^2 , the net rate of entropy generation rises.

5 | CONCLUSIONS

In the current study, effects of fluid entrance temperatures and various heat fluxes on thermo hydraulic performance of a MCHS have been examined experimentally. The experiment was conducted for different flow rates (0.1-0.5 L/min), Reynolds number ($80 < Re < 450$), different entrance temperature (20°C - 40°C) and heat flux of 50 and 66.7 W/cm^2 . The main outcomes of this study are followed:

1. Increase in nanoparticle addition into the base fluid, Reynolds number, fluid inlet temperature and heat flux have major influence on Nusselt number (Nu) and fluid heat transfer coefficient (h). Optimum enhancement was observed to be 30.93% for graphene/water nanofluid over base fluid, due to its higher thermal conductivity. An improvement of 3.9%-6.8% occurred when fluid entrance temperature raised from 20 to 40°C for all the coolants. Whereas, h rises within the range of 1.9%-5.1%, when heat flux rises from 50 to 66.7 W/cm^2 .
2. There was a penalty in terms of pressure drop and pumping power by the suspension of nanoparticles

due to increment in density and viscosity. Fluid inlet temperature and heat flux both have negative consequences on pressure drop. Pressure drop reduces with fluid entrance temperature when it increases from 20°C to 40°C. Reynolds number has disadvantageous impact on friction factor.

3. Al_2O_3 + graphene/water hybrid nanofluid yields maximum value of comparison factor ($h/\Delta p$) among all other fluids used.
4. In all working conditions, *PEC* value is found greater than unity. This indicates that using nanofluid can be considered a better option as a coolant in MCHS.
5. Graphene/water nanofluid is superior in *HTC* enhancement but has less comparison factor ($h/\Delta p$) as compared to Al_2O_3 + graphene-based hybrid nanofluid and Al_2O_3 nanofluid.
6. Hybrid nanofluid with different shape and size of nanoparticles have favourable comparison factor ($h/\Delta p$) compared to mono nanofluids and hybrid nanofluid of similar particles.
7. The total rate of entropy generation is higher for graphene/water nanofluid but at higher Reynolds number it stagnated. Al_2O_3 + graphene/water hybrid nanofluid has lower value of total entropy generation rate among all other working fluids.

ACKNOWLEDGEMENT

Authors want to acknowledge the research support provided by Indian institute of Technology (BHU), Varanasi, 221005, India.

NOMENCLATURE

A_b	base area (m^2)
A	effective MCHS area for heat transfer (m^2)
c_p	specific heat capacity (J/kg K)
d_h	hydraulic diameter (mm)
f	friction factor
h	convective heat coefficient ($\text{W}/\text{m}^2 \text{K}$)
h_{ch}	height of minichannel (mm)
J	comparison factor ($\text{m}/\text{s K}$)
k	thermal conductivity ($\text{W}/\text{m K}$)
\dot{V}	volumetric coolant flow rate (L/min)
Nu	Nusselt number
Δp	pressure drop (Pa)
Pr	Prandtl number
\dot{Q}	heat transfer rate (W)
Re	Reynolds number
T	fluid temperature ($^\circ\text{C}$)
u	fluid velocity (m/s)
v, vol	volume
W	width of heat sink (mm)
L	length of heat sink (mm)
w_{ch}	width of channel (mm)

<i>HTC</i>	heat transfer coefficient
<i>IEP</i>	isoelectric point
L_{ch}	length of channel (mm)
<i>MCHS</i>	minichannel heat sink
<i>PCM</i>	phase change material
<i>PEC</i>	performance evaluation criteria
S_{gen}	total rate of entropy generation (W/K)
T_{tc}	surface temperature
k_s	heat sink conductivity (W/m K)

GREEK SYMBOLS

μ	fluid dynamic viscosity (Pa s)
ρ	density of fluid (kg/m^3)
Φ	nanofluid volume concentration

SUBSCRIPTS

bf	base fluid
ch	channel
np	nanoparticles
hnf	hybrid nanofluid
in	inlet
out	outlet
w	wall
m	mean

DATA AVAILABILITY STATEMENT

Data sharing is not applicable to this article as no new data were created or analyzed in this study.

ORCID

Wasim Jamshed  <https://orcid.org/0000-0001-9438-6132>
Kottakkaran Soopy Nisar  <https://orcid.org/0000-0001-5769-4320>

REFERENCES

1. Ndao S, Peles Y, Jensen MK. Multi-objective thermal design optimization and comparative analysis of electronics cooling technologies. *Int J Heat Mass Transf.* 2009;52:4317-4326.
2. Vajravel LV, Swaminathan SK, Baskaran S, Sekar RK. Experimental investigations on heat transfer in a new minichannel heat sink. *Int J Therm Sci.* 2019;140:144-153.
3. Ahuja AS. Augmentation of heat transport in laminar flow of polystyrene suspensions. I Experiments and results. *J Appl Phys.* 1975;46(8):3408-3416.
4. Sonawane T, Patil P, Abhay C, Dusane BM. A review on heat transfer enhancement by passive methods. *Int Res J Eng Technol.* 2016;03(09):1567-1574.
5. Dewan A, Mahanta P, Sumithra Raju K, Suresh Kumar P. Review of passive heat transfer augmentation techniques. *Proc Inst Mech Eng A J Power Energy.* 2004;218(7):509-527.
6. Mahesh J, Rahul A, Diksha B, Amol B, Mayura M. Review on enhancement of heat transfer by active method. *Int J Curr Eng Technol.* 2016;(06):221-225.

7. Al-Sallami W, Al-Damook A, Thompson HM. A numerical investigation of thermal airflows over strip fin heat sinks. *Int Commun Heat Mass Transf.* 2016;75:183-191.
8. Al-Damook A, Kapur N, Summers JL, Thompson HM. An experimental and computational investigation of thermal air flows through perforated pin heat sinks. *Appl Therm Eng.* 2015;89:365-376.
9. Al-Damook A, Alkasmoul FS. Heat transfer and airflow characteristics enhancement of compact plate-pin fins heat sinks – a review. *Propul Power Res.* 2018;7:138-146.
10. Al-Sallami W, Al-Damook A, Thompson HM. A numerical investigation of the thermal-hydraulic characteristics of perforated plate fin heat sinks. *Int J Therm Sci.* 2017;121:266-277.
11. Ghani IA, Sidik NAC, Kamaruzaman N. Hydrothermal performance of microchannel heat sink: the effect of channel design. *Int J Heat Mass Transf.* 2017;107:21-44.
12. Whitesides GM. The origins and the future of microfluidics. *Nature.* 2006;442:368-373.
13. Babar H, Ali HM. Towards hybrid nanofluids: preparation, thermophysical properties, applications, and challenges. *J Mol Liq.* 2019;281:598-633.
14. Tiwari AK, Ghosh P, Sarkar J. Particle concentration levels of various nanofluids in plate heat exchanger for best performance. *Int J Heat Mass Transf.* 2015;89:1110-1118.
15. Arshad A, Jabbar M, Yan Y. David Reay a review on graphene based nanofluids: preparation, characterization and applications. *J Mol Liq.* 2019;279:444-484.
16. Nakharintr L, Naphon P, Wiriyasart S. Effect of jet-plate spacing to jet diameter ratios on nanofluids heat transfer in a minichannel heat sink. *Int J Heat Mass Transf.* 2018;116:352-361.
17. Ho CJ, Liao JC, Li CH, Yan WM, Amani M. Experimental study of cooling performance of water-based alumina nanofluid in a minichannel heat sink with MEPCM layer embedded in its ceiling. *Int Commun Heat Mass Transf.* 2019;103:1-6.
18. Nikkhah V, Nakhjavani SH. Thermal performance of a micro heat exchanger (MHE) working with zirconia-based nanofluids for industrial cooling. *Int J Indus Chem.* 2019;10:193-204. <https://doi.org/10.1007/s40090-019-0183-6>
19. Al-Rashed AAAA, Shahsavar A, Entezari S, Moghimi MA, Adio SA, Nguyen TK. Numerical investigation of non-Newtonian water-CMC/CuO nanofluid flow in an offset strip-fin microchannel heat sink: thermal performance and thermodynamic considerations. *Appl Therm Eng.* 2019;155:247-258.
20. Sajid MU, Ali HM, Bicer Y. Exergetic performance assessment of magnesium oxide–water nanofluid in corrugated minichannel heat sinks: an experimental study. *Int J Energy Res.* 2020;1-17. <https://doi.org/10.1002/er.6024>.
21. Fadhil AM, Khalil WH, Al-Damook A. The hydraulic-thermal performance of miniature compact heat sinks using SiO₂-water nanofluids. *Heat Transf Asian Res.* 2019;48:1-14. <https://doi.org/10.1002/htj.21532>
22. Hatami M, Ganji DD. Thermal and flow analysis of microchannel heat sink (MCHS) cooled by cu–water nanofluid using porous media approach and least square method. *Energy Conver Manage.* 2014;78:347-358.
23. Ho CJ, Chen WC, Yan WM. Correlations of heat transfer effectiveness in a minichannel heat sink with water-based suspensions of Al₂O₃ nanoparticles and/or MEPCM particles. *Int J Heat Mass Transf.* 2014;69:293-299.
24. Ho CJ, Chen WC, Yan WM. Experiment on thermal performance of water-based suspensions of Al₂O₃ nanoparticles and MEPCM particles in a minichannel heat sink. *Int J Heat Mass Transf.* 2014;69:276-284.
25. Ho CJ, Chen WC, Yan WM, Amani P. Contribution of hybrid Al₂O₃-water nanofluid and PCM suspension to augment thermal performance of coolant in a minichannel heat sink. *Int J Heat Mass Transf.* 2018;122:651-659.
26. Selvakumar P, Suresh S. Use of Al₂O₃-Cu/water hybrid nanofluid in an electronic heat sink. *IEEE Trans Compon Packag Manuf Technol.* 2012;2:1600-1607.
27. Ahammed N, Asirvatham LG, Wongwises S. Entropy generation analysis of graphene–alumina hybrid nanofluid in multiport minichannel heat exchanger coupled with thermoelectric cooler. *Int J Heat Mass Transf.* 2016;103:1084-1097.
28. Hussien AA, Yusop MZNM, Al-Kouz W, Mahmoudi E, Mehrali M. Heat transfer and entropy generation abilities of MWCNTs/GNPs hybrid nanofluids in microtubes. *Entropy.* 2019;21(480):1-17. <https://doi.org/10.3390/e21050480>
29. Hussien AA, Yusop NM, Al-Nimr MA, Abdullah MZ, Janvekar AA, Elnaggar MH. Numerical study of heat transfer enhancement using Al₂O₃-graphene/water hybrid nanofluid flow in mini tubes. *Iran J Sci Technol A.* 2019;43:1989-2000. <https://doi.org/10.1007/s40995-018-0670-1>
30. Nimmagadda R, Venkatasubbaiah K. Experimental and multiphase analysis of nanofluids on the conjugate performance of micro-channel at low Reynolds numbers. *Heat Mass Transf.* 2017;53:2099-2115.
31. Bahiraei M, Berahmand M, Shahsavar A. Irreversibility analysis for flow of a non-Newtonian hybrid nanofluid containing coated CNT/Fe₃O₄ nanoparticles in a minichannel heat exchanger. *Appl Therm Eng.* 2017;125:1083-1093.
32. Bahiraei M, Heshmatian S. Thermal performance and second law characteristics of two new microchannel heat sinks operated with hybrid nanofluid containing graphene–silver nanoparticles. *Energy Conver Manage.* 2018;168:357-370.
33. Goodarzi M, Tlili I, Tian Z, Safaei M. Efficiency assessment of using graphene nanoplatelets-silver/water nanofluids in microchannel heat sinks with different crosssections for electronics cooling. *Int J Numer Method.* 2019;30:347-372. <https://doi.org/10.1108/HFF-12-2018-0730>
34. Bahiraei M, Mazaheri N. Application of a novel hybrid nanofluid containing graphene–platinum nanoparticles in a chaotic twisted geometry for utilization in miniature devices: thermal and energy efficiency considerations. *Int J Mech Sci.* 2018;138–139:337-349.
35. Shahsavar A, Godini A, Sardari PT, Toghraie D, Salehipour H. Impact of variable fluid properties on forced convection of Fe₃O₄/CNT/ water hybrid nanofluid in a double-pipe minichannel heat exchanger. *J Therm Anal Calorim.* 2019;137:1031-1043.
36. Uysal C, Gedik E, Chamkha AJ. A numerical analysis of laminar forced convection and entropy generation of a diamond-Fe₃O₄/water hybrid nanofluid in a rectangular minichannel. *J Appl Fluid Mech.* 2019;12:391-402.
37. Ho CJ, Liu YC, Ghalambaz M, Yan WM. Forced convection heat transfer of Nano-encapsulated phase change material (NEPCM) suspension in a mini-channel heatsink. *Int J Heat Mass Transf.* 2020;155:119858.

38. Kumar V, Sarkar J. Numerical and experimental investigations on heat transfer and pressure drop characteristics of Al_2O_3 - TiO_2 hybrid nanofluid in minichannel heat sink with different mixture ratio. *Powder Technol.* 2019;345:717-727.
39. Kumar V, Sarkar J. Particle ratio optimization of Al_2O_3 -MWCNT hybrid nanofluid in minichannel heat sink for best hydrothermal performance. *Appl Therm Eng.* 2020;165:114546.
40. Sarafraz MM, Safaei MR, Tian Z, Goodarzi M, Pedone E, Filho MAB. Thermal assessment of nano-particulate graphene water/ethylene glycol (WEG 60:40) nano-suspension in a compact heat exchanger. *Energies.* 2019;12:1-12.
41. Sarafraz MM, Arya H, Arjomandi M. Thermal and hydraulic analysis of a rectangular microchannel with gallium-copper oxide nano-suspension. *J Mol Liq.* 2018;263:382-389.
42. Sarafraz MM, Goodarzi M, Yang B, Arjomandi M. Heat transfer analysis of Ga-in-Sn in a compact heat exchanger equipped with straight micro-passages. *Int J Heat Mass Transf.* 2019;139:675-684.
43. Sarafraz MM, Hart J, Shrestha E, Arya H, Arjomandi M. Experimental thermal energy assessment of a liquid metal eutectic in a microchannel heat exchanger equipped with a (10 Hz/50 Hz) resonator. *Appl Therm Eng.* 2019;148:578-590.
44. Ellahi R, Hussain F, Abbas SA, Sarafraz MM, Goodarzi M, Shadloo MS. Study of two-phase Newtonian nanofluid flow hybrid with hafnium particles under the effects of slip. *Inventions.* 2020;5(1):1-22.
45. Nazari S, Ellahi R, Sarafraz MM, Safaei MR, Asgari A, Akbari OA. Numerical study on mixed convection of a non-Newtonian nanofluid with porous media in a two lid-driven square cavity. *J Therm Anal Calor.* 2020;140:1121-1145.
46. Pourmehran O, Sarafraz MM, Rahimi-Gorji M, Ganji DD. Rheological behaviour of various metal-based nano-fluids between rotating discs: a new insight. *J Taiwan Inst Chem Eng.* 2018;88:37-48.
47. Sarafraza MM, Aryab H, Saeedia M, Ahmadi D. Flow boiling heat transfer to MgO-therminol 66 heat transfer fluid: experimental assessment and correlation development. *Appl Therm Eng.* 2018;138:552-562.
48. Bhattad A, Sarkar J. Effects of nanoparticle shape and size on the thermohydraulic performance of plate evaporator using hybrid nanofluids. *J Therm Anal Calorim.* 2021;143:767-779.
49. Gao W, Zhang JF, Qu ZG, Tao WQ. Numerical investigations of heat transfer in hybrid microchannel heat sink with multi-jet impinging and trapezoidal fins. *Int J Therm Sci.* 2021;164:106902.
50. Maddah H, Aghayari R, Mirzaee M, Ahmadi MH, Sadeghzadeh M, Chamkha AJ. Factorial experimental design for the thermal performance of a double pipe heat exchanger using Al_2O_3 - TiO_2 hybrid nanofluid. *Int Commun Heat Mass Transf.* 2018;97:92-102.
51. Sajid MU, Ali HM, Sufyan A, Rashid D, Zahid SU, Rehman WU. Experimental investigation of TiO_2 -water nanofluid flow and heat transfer inside wavy mini-channel heat sinks. *J Therm Anal Calorim.* 2019;137:1279-1294.
52. Ho CJ, Chen WC. An experimental study on thermal performance of Al_2O_3 /water nanofluid in a minichannel heat sink. *Appl Therm Eng.* 2013;50:516-522.
53. Cheng H, Lei H, Dai C. Thermo-hydraulic characteristics and second-law analysis of a single-phase natural circulation loop with end heat exchangers. *Int J Therm Sci.* 2018;129:375-384.
54. Kumar V, Sarkar J. Experimental hydrothermal characteristics of minichannel heat sink using various types of hybrid nanofluids. *Adv Powder Technol.* 2020;31:621-631.
55. Kline SJ, McClintock FA. Describing uncertainties in single-sample experiments. *Mech Eng.* 1953;75:3-8.
56. Jiang PX, Fan MH, Si GS, Ren ZP. Thermal-hydraulic performance of small-scale micro-channel and porous-media heat-exchangers. *Int J Heat Mass Transf.* 2001;44:1039-1051.
57. Moraveji MK, Ardehali RM. CFD modeling (comparing single and two-phase approaches) on thermal performance of Al_2O_3 /water nanofluid in mini-channel heat sink. *Int Commun Heat Mass Transf.* 2013;44:157-164.
58. Peng XF, Peterson GP, Wang BX. Frictional flow characteristics of water flowing through rectangular microchannels. *Exp Heat Transf.* 1994;7:249-264.
59. Sarafraz MM, Yang B, Pourmehran O, Arjomandi M, Ghomashchi R. Fluid and heat transfer characteristics of aqueous graphene nanoplatelet (GNP) nanofluid in a microchannel. *Int Commun Heat Mass Transf.* 2019;107:24-33.
60. Das SK, Choi SUS, Patel HE. Heat transfer in Nanofluids—a review. *Heat Transf Eng.* 2006;27:3-19.

How to cite this article: Kumar V, Singh SK, Kumar V, Jamshed W, Nisar KS. Thermal and thermo-hydraulic behaviour of alumina-graphene hybrid nanofluid in minichannel heat sink: An experimental study. *Int J Energy Res.* 2021;1-15. <https://doi.org/10.1002/er.7134>